International Journal of Pharmaceutics: X 6 (2023) 100194

Contents lists available at ScienceDirect

International Journal of Pharmaceutics: X

journal homepage: www.sciencedirect.com/journal/international-journal-of-pharmaceutics-x

Formulation, optimization, in-vivo biodistribution studies and histopathological safety assessment of duloxetine HCl-loaded ultra-elastic nanovesicles for antidepressant effect after intranasal and transdermal delivery

Radwa M.A. Abd-Elal [a,**], Aya M. Essawy [b], Maha A. Salem [c], Mahitab Elsayed [b], Mona G. Khalil [c], Eman Abdelhakeem [d], Nouran A. Ali [d], Mai Ahmed Tawfik [d,*]

[a] Pharmaceutics and Drug Manufacturing Department, Faculty of pharmacy, Modern University for Technology and Information (MTI), Cairo 11571, Egypt
[b] Department of Clinical Pharmacy, Faculty of pharmacy, Modern University for Technology and Information (MTI), Cairo 11571, Egypt
[c] Department of Pharmacology and Toxicology, Faculty of pharmacy, Modern University for Technology and Information (MTI), Cairo 11571, Egypt
[d] Department of Pharmaceutics and Industrial Pharmacy, Faculty of Pharmacy, Cairo University, Cairo, Egypt

ARTICLE INFO

Keywords:
Duloxetine hydrochloride
Elastosomes
Histopathology
Intranasal
In-vivo studies
Transdermal

ABSTRACT

Duloxetine hydrochloride (DUL) is a BCS class-II antidepressant drug, acting via serotonin and norepinephrine reuptake inhibition. Despite high oral absorption, DUL suffers limited bioavailability due to extensive gastric and first-pass metabolism. To improve DUL's bioavailability; DUL-loaded elastosomes were developed, via full factorial design, utilizing various span®60: cholesterol ratios, edge activator types and amounts. Entrapment efficiency (E.E.%), particle size (PS), zeta potential (ZP) and in-vitro released percentages after 0.5 h ($Q_{0.5h}$) and 8 h (Q_{8h}) were evaluated. Optimum elastosomes (DUL-E1) were assessed for morphology, deformability index, drug crystallinity and stability. DUL pharmacokinetics were evaluated in rats following intranasal and transdermal application of DUL-E1 elastosomal gel. DUL-E1 elastosomes [comprising span®60 and cholesterol (1:1) and brij S2 (edge activator; 5 mg)] were optimum with high E.E.% (81.5 ± 3.2%), small PS (432 ± 13.2 nm), ZP (−30.8 ± 3.3 mV), acceptable $Q_{0.5h}$ (15.6 ± 0.9%), and high Q_{8h} (79.3 ± 3.8%). Intranasal and transdermal DUL-E1 elastosomes revealed significantly higher C_{max} (251 ± 18.6 and 248 ± 15.9 ng/mL) at T_{max} (2 and 4 h) and improved relative bioavailability (≈ 2.8 and 3.1 folds) respectively, in comparison to oral DUL aqueous solution. In-vivo histopathological studies were conducted to ensure the safety of DUL-E1. Elastosomes are promising novel nano-carriers, capable of enhancing the bioavailability of DUL via various routes of administration.

1. Introduction

Depression is the most serious disabling mental disorder, negatively affecting the psychological as well as the physical health (Tawfik et al., 2020). Depression influences about 264 million people, and is responsible for about 60% of the suicidal incidences worldwide (Nemeroff, 2007; Rana et al., 2020). Commonly administered antidepressant treatments; tricyclic antidepressants (first generation), selective serotonin reuptake inhibitors, dopamine reuptake inhibitors, and norepinephrine reuptake inhibitors (2nd generation) suffer various limitations and have many side effects (Khatoon et al., 2019; Tawfik et al., 2021). Consequently, more efficacious, safer, and better-tolerated pharmacological treatments of depression are needed.

Duloxetine hydrochloride (DUL; (3*S*)-*N*-methyl-3-naphthalen-1-yloxy-3-thiophen-2ylpropan-1-amine) is considered a novel antidepressant drug acting via a dual mechanism, being selective serotonin as well as norepinephrine reuptake inhibitor (Salem et al., 2022). It was reported that DUL shows higher potency, more efficacy, and less toxicity compared to other antidepressant drugs (Khatoon et al., 2019; Setia et al., 2013). Although DUL shows high oral absorption (Elsenosy et al., 2020), variable poor bioavailability (≈ 40%) is achieved due to the extensive degradation in the acidic medium of the gastrointestinal tract

* Correspondence to: M A Tawfik, Cairo University, Kasr El-Aini Street, Cairo 11562, Egypt.
** Correspondence to: R M A Abd-Elal, Modern University for Technology and Information (MTI), Cairo 11571, Egypt.
E-mail addresses: radwa.mahrous@pharm.mti.edu.eg (R.M.A. Abd-Elal), mai.tawfik@pharma.cu.edu.eg (M.A. Tawfik).

https://doi.org/10.1016/j.ijpx.2023.100194
Received 2 May 2023; Received in revised form 10 June 2023; Accepted 22 June 2023
Available online 24 June 2023

and first-pass metabolism via the hepatic cytochrome P450 P1A2 (El Sharawy et al., 2017; Salem et al., 2022). DUL, a BCS class-II drug, is considered a promising candidate for intranasal, as well as transdermal drug delivery, due to its physicochemical properties including lipophilicity (log $P = 4.2$) and molecular weight (330 g/mol) (Peddapalli et al., 2018).

Intranasal administration is a fast, potential drug delivery route that enhances the delivery of various drugs to the brain, bypassing the blood-brain barrier as well as enzymatic and hepatic metabolism (Elsenosy et al., 2020; Khatoon et al., 2019; Yasir et al., 2022b). Nasal delivery is an attractive route of drug administration owing to non-invasiveness, fast onset of action, improved bioavailability and ease of administration (Abd-Elal et al., 2016; El Taweel et al., 2021; Yasir et al., 2021).

Transdermal administration is also a promising alternative drug delivery route for various drugs, suffering from high dosing frequency, extensive gastrointestinal and first-pass metabolism (Zafar et al., 2022b; Tawfik et al., 2023). Transdermal drug delivery improves the bioavailability, via delivering the drugs at a predetermined controlled manner and improves the patient compliance owing to being painless, reduced side effects, and dosing frequency (Aziz et al., 2018; Hassan et al., 2022).

Elastosomes (ultra-elastic nanovesicles) are of the most novel and promising nano-vesicular drug delivery systems. Owing to their ultra-elasticity, they were proved to enhance tissue penetration (Ali et al., 2021). Bilosomes (modified niosomes) are nano-vesicles comprising bile salts added to the conventional non-ionic amphiphiles (El Taweel et al., 2021). Recent publications stated that bilosomes succeeded to enhance the intranasal (El Taweel et al., 2021) as well as the transdermal (Ahmed et al., 2020) delivery of various drugs. Elastosomes were developed by modifying the composition of bilosomes, through the addition of different edge activator (EA) types. Owing to the surface tension lowering properties of both bile salts as well as EAs, elastosomes are considered to be of greater deformability, in comparison to bilosomes (Aziz et al., 2018; Mosallam et al., 2021). Being ultra-elastic, elastosomes squeeze themselves through the pores of the nasal mucosa as well as the skin to reach deeper tissues. Elastosomes can enhance tissue penetration via modifying the nasal mucosa and the stratum corneum (Ali et al., 2021; El Taweel et al., 2021).

Various previous trials were conducted to overcome DUL's limitations. El Sharawy et al. (2017), and Peddapalli et al. (2018) developed DUL-loaded buccal films and buccal tablets respectively. Setia et al. (2013) aimed to surpass the acidic drug degradation by preparing DUL-loaded enteric coated mucoadhesive microspheres. Also, Khatoon et al. (2019) chose the intranasal drug delivery route, for DUL brain targeting and avoiding the hepatic metabolism. The rectal route was also explored by Salem et al. (2022) for improving the bioavailability of DUL.

Our current work aims to develop and characterize DUL-loaded elastosomes to enhance the bioavailability of DUL. Elastosomes were developed using vesicle forming material (cholesterol; CH), along with surfactant (span®60), in the presence of bile salt (sodium deoxycholate; SDC), and different edge activators (EAs). Two span®60: cholesterol ratios (1:1 or 5:1), two EA types (brij S2 or cremophor RH 40); at two different amounts (5 or 10 mg) were investigated. The optimum developed elastosomes (with respect to the in-vitro characterization studies) were promoted for in-vivo histopathological safety assessment as well as in-vivo bio-distribution studies in rats after intranasal and transdermal delivery.

The novelty of our study relies on the fact that elastosomal DUL have not been investigated before. Furthermore, previous studies explored the effect of the type as well as the amount of edge activator on the characteristics of the developed elastosomes (Aziz et al., 2018; Mosallam et al., 2021), however the factor Span® 60: cholesterol ratio was not studied before. On the other hand, in-vivo biodistribution studies were conducted via two routes (intranasal and transdermal delivery) to compare and choose the optimum one, beside in-vivo histopathological studies were carried out on different organs (heart, liver, and brain) to ensure the safety of the new systems and that no marked histopathological changes were found.

2. Materials and methods

2.1. Materials

Duloxetine hydrochloride (DUL), reboxetine (internal standard; IS) were kindly donated by EVA Pharma (Cairo, Egypt). Cholesterol (CH), sodium deoxycholate (SDC), acetonitrile (HPLC grade), brij S2 (polyoxyethylene (2) stearyl ether), span®60 (sorbitan monostearate), and Spectra Por© dialysis tubing (Mol. Wt cut off 12–14 g/mol) were bought from Sigma-Aldrich® (St. Louis, MO). Cremophor RH 40 was procured from BASF Co. (Florham Park, NJ). Chloroform, potassium dihydrogen phosphate, methanol, and sodium chloride, disodium hydrogen phosphate were acquired from El-Nasr Pharmaceutical Chemicals Co. (Cairo, Egypt). Hydroxypropyl methylcellulose (HPMC) K4M was brought from Dow Chemical Company (Midland, US). All other (analytical grade) reagents were used as provided.

2.2. Methodology

2.2.1. Development of DUL-loaded elastosomes

Thin film hydration technique was adopted for the development of eight DUL-loaded elastosomes, comprising vesicle forming material (CH), surfactant (span®60), bile salt (SDC), and edge activator (EA), with slight modifications (Aziz et al., 2018; Dai et al., 2013). The investigated variables were span®60: CH ratio (1:1 or 5:1), EA type (brij S2 or cremophor RH 40) as well as EA amount (5 or 10 mg). In a round-bottom flask (500 mL); drug (20 mg), along with the elastosomal components (span®60, CH; 20 mg, SDC;5 mg and EA) were completely dissolved in 10 mL organic solvent mixture of chloroform/methanol (7:3, % *v*/v) using bath sonicator (Crest Ultrasonics Corp., Trenton, NJ) (Mosallam et al., 2021). Utilizing a rotatory evaporator; DUL-loaded clear organic solution was evaporated slowly (Heidolph VV 2000, Burladingen, Germany) at 60 °C, under vacuum to form a clear dry film, at 120 rpm for 30 min. Then, the obtained film was hydrated with distilled water (10 mL), using the same apparatus, while revolving under normal pressure, at 120 rpm for 1 h. Finally, the developed vesicles were bath-sonicated for 30 min to reduce their size and were kept overnight at 4 °C to equilibrate. For comparative study, DUL-loaded bilosomes, comprised of span®60: CH (1:1) along with SDC (5 mg) in the absence of EA, were prepared by the same technique.

2.2.2. In-vitro characterization of DUL-loaded elastosomes

2.2.2.1. DUL entrapment efficiency percentage (E.E.%). The indirect technique was adopted via measuring the unentrapped DUL concentration of each elastosomal dispersion (Aziz et al., 2018). Free DUL was separated from the developed dispersions by ultra-centrifugation (22,000 rpm) at 4 °C for 1 h (Heraeus Megafuge 1.0 R; Hanau, Germany). Diluted supernatants were analyzed for unentrapped DUL concentrations (Shimadzu UV-1601 PC spectrophotometer, Kyoto, Japan) at λ_{max} 286 nm (Elsenosy et al., 2020). E.E.% values were calculated according to the following equation. Three independent measurements were utilized for the calculation of the mean ± S.D.

$$\text{E.E.\%} = \frac{\text{Total theoritical amount of DUL (mg)} - \text{Amount of unentrapped DUL (mg)}}{\text{Total theoritical amount of DUL (mg)}} \times 100 \quad (1)$$

2.2.2.2. Particle size (PS), polydispersity index (PDI), and zeta potential (ZP). PS and PDI measurements were conducted at 25 °C, via quasi-elastic light scattering technique using Zetasizer Nano ZS (Malvern instruments; Worcestershine, UK) (Abd-Elal et al., 2016). To develop appropriate intensity of light scattering, DUL-loaded elastosomal dispersions were adequately diluted (15 folds) before measurements at 25 °C. Homogenous distribution of PS could be revealed by low PDI values (Tawfik et al., 2021). The physical stability could be determined by measuring the electrophoretic mobility (ZP values) of the charged DUL-loaded elastosomes using a laser doppler anemometer, connected to the same equipment. Results were presented as mean ($n = 3$) ± S.D.

2.2.2.3. In-vitro release studies. The membrane diffusion technique was adopted for the determination of the in-vitro release profiles of DUL from the developed elastosomes. Aliquots of DUL-loaded elastosomes (equivalent to 5 mg DUL) were transferred to soaked semi-permeable cellulose dialysis membrane. Following loading, the membrane tubing was clamped and immersed in the release medium; phosphate buffer saline (PBS; pH 7.4, 50 mL), in a shaking water bath (Unimax, IKA, Staufen, Germany) maintained at 50 strokes per min and 37 ± 0.5 °C (Elsenosy et al., 2020). For the purpose of maintaining sink conditions, replacement by fresh PBS was carried out after each sample (3 mL) withdrawal, at pre-defined time points up to 8 h (0.5, 1, 2, 4, 6, and 8 h). DUL concentrations were analyzed spectrophotometrically at λ_{max} 286 nm. DUL released percentages were plotted versus their corresponding time points. Percentages of DUL released after 0.5 h ($Q_{0.5h}$) and 8 h (Q_{8h}) were determined for comparison and optimization. Parallelly, in-vitro release profile of DUL from an aqueous DUL solution was similarly conducted, to ensure that dialysis membrane didn't cause any retardation of drug release. Presented results were the average (± S.D.) of three experiments.

2.2.3. Statistical design and optimization of DUL-loaded elastosomes via 2^3 full factorial design

The statistical significance of the developed DUL-loaded elastosomes was performed via a full factorial (2^3) design, utilizing Design-Expert® software version 7 (Stat-Ease, Inc., Minneapolis, MN). The evaluation of three factors; X_1: Span® 60: CH ratio, X_2: EA type and X_3: EA amount (each at two levels) was performed in this design; Table 1. The responses were E.E.% (Y_1), PS (Y_2), ZP (Y_3), $Q_{0.5h}$ (Y_4) and Q_{8h} (Y_5). The desirability values were assessed for optimization, where constraints were adjusted to minimize PS, while maximize E.E.%, ZP (absolute value), $Q_{0.5h}$ and Q_{8h}. One-way ANOVA ($p < 0.05$) was conducted to test the statistical significance of each of the three factors on the chosen responses and to select the optimum DUL-loaded elastosomes which were subjected to further studies.

Table 1
Design parameters and response's constraints of 2^3 full factorial design of DUL-loaded elastosomes.

Independent Variables	Level of Variables	
	(−1)	(+1)
X_1: Span®60: CH ratio	1:1	5:1
X_2: EA Type	Brij S2	Cremophor RH 40
X_3: EA Amount (mg)	5	10
Response's Constraints		
Y_1: E.E. * (%)	Maximize	
Y_2: PS (nm)	Minimize	
Y_3: ZP (mV)	Maximize (as absolute values)	
Y_4: $Q_{0.5h}$ (%)	Maximize	
Y_5: Q_{8h} (%)	Maximize	

2.2.4. Characterization of the optimum DUL-loaded elastosomes

2.2.4.1. Transmission electron microscopy (TEM). TEM (Joel JEM 1230, Tokyo, Japan) was utilized for visualizing the morphologic properties and topographic characteristics of the optimum DUL-loaded elastosomes, after proper dilution and negative staining with (2% *w/v*) phosphotungestic acid. Briefly, two drops of the diluted elastosomal dispersion were stratified onto a copper grid (carbon-coated), stained with a drop of phosphotungestic acid solution, and left to air-dry before visualization at 80 kV (Abd-Elal et al., 2016; Tawfik et al., 2018).

2.2.4.2. Deformability index (DI). The elasticity of the optimum DUL-loaded elastosomes was assessed via the extrusion technique, in comparison to the corresponding DUL-loaded bilosomes formulation (Aziz et al., 2018; Van den Bergh et al., 2001). Firstly, both elastosomal and bilosomal dispersions were (10-folds) diluted. Using air compressor under 2.5 bar pressure (Haug Kompressoren AG; B€uchi Labortechnik AG, Flawil, Switzerland), diluted dispersions were extruded through 200 nm pore size nylon filters (Jinteng Experiment Equipment Co., Ltd., Tianjin, China) (El Zaafarany et al., 2010; Lei et al., 2013). Presented results were the means (± SD) of three independent experiments. According to the mentioned equation; DI values were estimated (Gupta et al., 2005):

$$DI = J\left(r_v/r_p\right)^2 \quad (2)$$

where J is considered to be weight of the extruded dispersion within 10 min, r_v is considered to be the particle size (PS; nm) of the vesicles after extrusion, and r_p is considered to be the pore size (nm) of the barrier.

2.2.4.3. Solid-state characterization study via differential scanning calorimetry (DSC). The optimum developed DUL-loaded elastosomes were freshly prepared, frozen, and lyophilized (−45 °C, 24 h) under (7×10^{-2} mbar) reduced pressure (Novalyphe-NL 500 lyophilizer, Savant Instruments; NY). The lyophilized elastosomes were subjected to the following characterization study.

DSC thermograms of pure DUL, CH, span® 60, SDC, EA (brij S2), physical mixture of all components, and the optimum developed DUL-loaded elastosomes were assessed (Shimadzu DSC-60, Shimadzu, Kyoto, Japan) using (99.9%) purified indium as reference. Each sample was heated from 30 to 300 °C in flat aluminum pans at a rate of 10 °C/min under nitrogen flow (30 mL/min) (Abd-Elal et al., 2020).

2.2.4.4. Effect of short-term storage after 3 months. For comparative purpose to elucidate the effect of storage on the characterization of DUL-loaded elastosomes, portions of the optimum elastosomal dispersions were stored in tightly-sealed glass vials in refrigerator (5 ± 2 °C) and other portions were kept on the shelf at room temperature (25 ± 2 °C) for 3 months (Desai et al., 2011). After the end of the storage period, both portions were compared to freshly prepared elastosomes and were evaluated for E.E.%, PS, PDI, and ZP. The results were expressed as mean ± SD ($n = 3$). SPSS® software version 22 was utilized for testing the statistical significance by student *t*-test, where *P* values ≤0.05 were considered significant.

2.2.4.5. Development of DUL-loaded elastosomal gel. 0.5% *w/v* hydroxypropyl methylcellulose (HPMC) gel was prepared and kept overnight in the fridge to achieve clear hydrogel. DUL-loaded elastosomal gels were prepared via the incorporation of the optimum DUL-loaded elastosomes (DUL-E1) into the HPMC hydrogel at a ratio of 1:1.

2.2.4.5.1. In-vitro characterization of DUL-E1 gel

2.2.4.5.1.1. Determination of pH

pH of DUL-E1 gel was assessed after diluting 0.5 mL of the pre-mentioned gel with 4.5 ml of distilled water and stirring on a magnetic stirrer for 5 min. Following, the electrode was immersed in the diluted gel and was left to equilibrate for a minute. Three independent measurements were conducted (Fahmy et al., 2018).

2.2.4.5.1.2. Determination of the rheological constants

A cone and plate viscometer (Brookfield viscometer; type DVT-2) was utilized for determining the rheological properties of the investigated DUL-E1 gel. 0.5 ml of the investigated gel was added to the plate. The rate of shear was increased from 0.5 up to 100 min^{-1}. Results were determined and were used for applying power model equation: $\tau = K(\gamma)^n$ where τ is the symbol of shear stress, γ is the symbol of rate of shear, K is the symbol of consistency index and finally n is the symbol of flow index (El Taweel et al., 2021).

2.2.5. In-vivo DUL pharmacokinetic studies

2.2.5.1. Study design. Following the approval (PI-3145) of the Research Ethics Committee at the Faculty of Pharmacy Cairo University, the in-vivo pharmacokinetic studies were adopted in accordance with EU Directive 2010/63/EU for animal experiments to compare DUL's pharmacokinetics after the intranasal as well as the transdermal application of DUL-E1 gel system versus the oral intake of DUL aqueous solution (reference treatment). A randomized, three-treatment, one-period, parallel design was conducted.

2.2.5.2. Animals. Eighteen male Swiss albino rats (weighing 200–250 g) were obtained from and kept in the animal house (Faculty of Pharmacy, Cairo University, Egypt), under suitable environmental conditions, till the conduction of the experiment.

2.2.5.3. Treatment administration and sample collection. Rats were assigned, randomly, to each of the three groups (6 rats each). Test treatments were intranasally or transdermally applied, while reference treatment was orally administered; all at 5 mg/ kg doses. Specific volumes of the optimum DUL loaded-elastosomal (DUL-E1) gel were applied intranasally to the first group, using narrow tubes (diameter: 100 μm) connected to Hamilton syringes. For efficient transdermal application, the backs of the second group's rats were shaved properly, prior to applying the optimum DUL loaded elastosomal (DUL-E1) gel. Concerning the reference group, rats were administered equivalent doses of DUL aqueous solution orally. The rats' doses were calculated by applying the following equation (Reagan-Shaw et al., 2008).

$$\text{Human dose}\left(\frac{\text{mg}}{\text{kg}}\right) = \text{Animal dose}\left(\frac{\text{mg}}{\text{kg}}\right) * \left(\frac{\text{Animal km}}{\text{Human km}}\right) \quad (3)$$

Where, Km is the conversion factor (Km = 6 and 37 for rats and humans, respectively). Blood was collected in plastic tubes (EDTA-treated), at different sampling points (pre-dose, 0.5, 1, 2, 4, 6, 12, 24, 48 and 72 h). Collected blood samples were centrifuged (Centurion Scientific LTD. Centrifuge, West Sussex, UK) at 5000 rpm for 15 min to separate clear plasma. Plasma samples were frozen at −80 °C till being analyzed (Elsenosy et al., 2020; Tawfik et al., 2021).

2.2.5.4. Sample preparation. Triple Quadrupole LC/MS/MS mass spectrometer was utilized for the determination of DUL concentrations in the thawed plasma samples (Micromass, Manchester, United Kingdom), according to the technique developed by Elsenosy et al. (2020). 25 μL of reboxetine solutions (internal standard (IS); 5 mg/ mL) were added to plasma samples (0.5 mL). Briefly, DUL and IS were vortexed together for 5 min and extracted with organic solvent (ethyl acetate; 4 mL). For separation, the organic layers were centrifuged (Eppendorf centrifuge 5804 R, Hamburg, Germany) at 4000 rpm for 10 min, then concentrated via a vacuum concentrator (Eppendorf 5301, Hamburg, Germany) and dried. Prior to injection; reconstitution of the dried samples was conducted using 500 μL of the mobile phase (El Sharawy et al., 2017).

Table 2
Output data of 2^3 full factorial design of the developed DUL-loaded elastosomes.

Output	Responses				
	Y_1: E.E. * (%)	Y_2: PS (nm)	Y_3: ZP (mV)	Y_4: $Q_{0.5h}$ (%)	Y_5: Q_{8h} (%)
R^2	0.9678	0.9987	0.9643	0.9848	0.9947
Adjusted R^2	0.9373	0.9977	0.9375	0.9735	0.9908
Predicted R^2	0.8713	0.9948	0.8572	0.9395	0.979
Adequate precision	18.66	69.75	16.28	27.05	41.95
p value	0.0019	< 0.0001	0.0024	0.0004	< 0.0001
F value	40.13	1040.22	36.03	86.87	253.05
Press value	27.64	1030	51.34	10.54	8.86

2.2.5.5. LC-MS/MS analysis of DUL. The analysis was adopted according to a validated method for the quantitation of DUL in biological samples via liquid chromatography– tandem mass spectrometry (LC–MS/MS) using reboxetine as IS (El Sharawy et al., 2017; Elsenosy et al., 2020).

2.2.5.6. Instrumentation. Determination of DUL concentrations was achieved via detection on a triple Quadrupole LC/MS/MS mass spectrometer (Micromass, Manchester, United Kingdom). Detection of ions was conducted using Multiple Reaction Monitoring (MRM) mode (+ve ion mode) using an electrospray ionization source. The mass transitions of DUL and IS ions were *m/z* 298.1 → 154.2 and m/z 314.2 → 175.1, respectively. Analyst® Software Ver. 1.6 (AB Sciex Instruments, Ontario, Canada) was used for analyzing the data. A calibration curve (r^2 = 0.999) was constructed over DUL concentration from 0.1 to 250 ng/mL.

2.2.5.7. Chromatographic conditions. Analysis was adopted using a C_{18} column; 50 × 4.6 mm; PS: 5um (Phenomenex, USA). The isocratic mobile phase: a mixture of acetonitrile (80%) and 0.5% formic acid (20%) was pumped at 1 mL/ min flow rate (pump; LC-20AD).

2.2.5.8. Pharmacokinetic and statistical analyses. Mean DUL plasma concentration-time profiles (± SD) were plotted for the three treatments. Maximum DUL plasma concentration (C_{max}), time to reach C_{max} (t_{max}), half-life of elimination ($t_{1/2}$), mean residence time ($MRT_{0-\infty}$), area under the curve from zero to the last sampling point (AUC_{0-72}) and to infinity ($AUC_{0-\infty}$) were estimated by applying non-compartmental analysis using Kinetica® software version 5 (Thermo Fisher Scientific Inc., Minneapolis, MN, USA). The percentages relative bioavailability of the test treatments were calculated from $AUC_{(0-\infty)}$ value of each test treatment relative to the $AUC_{(0-\infty)}$ value of the reference treatment (Abd-Elal et al., 2016; Tawfik et al., 2019). Results were expressed as mean (±SD), but MRT and T_{max} were presented as median (range).

2.2.6. In-vivo DUL histopathological studies

At the end of the in-vivo pharmacokinetic studies, rats from the different groups were sacrificed; where group 1 and 2 received intranasal and transdermal application of DUL-E1 respectively, while group 3 was administered DUL aqueous solution orally. Autopsy samples were collected from different organs (heart, liver, and brain), excised and then fixed in 10% formalin solution. Specimens from different organs were

Table 3
Experimental runs, independent variables (formulation factors) and dependent variables (measured responses) of 2^3 full factorial design of the developed DUL-loaded elastosomes.

Formulae	Formulation Factors (Independent Variables)			Measured Responses (Dependent Variables)				
	X_1: Span®60: CH ratio	X_2: EA Type	X_3: EA Amount (mg)	Y_1: E.E. (%)	Y_2: PS (nm)	Y_3: ZP (mV)	Y_4: $Q_{0.5h}$ (%)	Y_5: Q_{8h} (%)
DUL-E1	1:1	Brij S2	5	81.5 ± 3.2	432 ± 13.2	−30.8 ± 3.3	15.6 ± 0.9	79.3 ± 3.8
DUL-E2	1:1	Brij S2	10	78.9 ± 2.1	398 ± 9.1	−37.3 ± 4.5	18.1 ± 2.8	85.8 ± 1.7
DUL-E3	1:1	Cremophor RH 40	5	77.2 ± 2.9	385 ± 21.5	−18.5 ± 1.4	22.9 ± 1.4	83.2 ± 1.7
DUL-E4	1:1	Cremophor RH 40	10	70.3 ± 4.1	353 ± 11.2	−22.7 ± 3.6	26.2 ± 1.5	88.7 ± 2
DUL-E5	5:1	Brij S2	5	88.9 ± 1.8	751 ± 17.3	−32.2 ± 2.2	10.4 ± 1.8	66.4 ± 0.8
DUL-E6	5:1	Brij S2	10	82.6 ± 2.2	693 ± 8	−39.4 ± 5.3	14.5 ± 0.9	72.1 ± 3.1
DUL-E7	5:1	Cremophor RH 40	5	80.4 ± 1.3	708 ± 16.2	−24.6 ± 2	16.3 ± 2.9	71.5 ± 1.9
DUL-E8	5:1	Cremophor RH 40	10	74.8 ± 3.7	661 ± 15.5	−28.4 ± 3.3	20.1 ± 1.4	75.3 ± 1.3
DUL-bilosomes	1:1	–	–	83.5 ± 3.5	365 ± 21.5	−30.2 ± 2.2	14.1 ± 2.8	76.2 ± 2.2

placed in blocks of paraffin beeswax, then cut (Leica Microsystems SM2400, Cambridge, UK), and put onto glass slides. Prior to electric light microscope observation; specimens were stained with hematoxylin and eosin (H&E) stains (Sharma et al., 2015; Vishwakarma et al., 2017).

3. Results and discussion

3.1. Development of DUL-loaded elastosomes

Elastosomes are ultra-elastic nano-vesicular drug carriers, revealing successful drug entrapment with high stability for various drugs especially lipophilic ones. Beside cholesterol, the main constituents of elastosomes are surfactant, bile salt and edge activator (Ali et al., 2021; Aziz et al., 2018; Mosallam et al., 2021). Eight DUL-loaded elastosomes were successfully developed via thin film hydration technique, using DUL, CH, span®60 (at a span®60: CH ratio of 1:1 or 5:1), EA (brij S2 or cremophor RH 40; 5 or 10 mg), and SDC. DUL-loaded bilosomes (at a span®60: CH ratio of 1:1, and EA free) were prepared via the same technique for comparative purpose (Table 3).

3.2. Factorial design outcomes

A full factorial design is a helpful tool for identifying the variables that potentially affect the developed system characterization. In our work, statistical analysis was performed using 2^3 full factorial design. The main model was selected. Signal to noise ratio was accurately measured to confirm that the navigation of the used model to the design space (Abd-Elal et al., 2020). Table 2 illustrated the output data, which demonstrated that the ratio of every response was >4. In addition, predicted R^2 was estimated to give a clear picture about a quality model (Mosallam et al., 2021). To be in rational agreement, the difference between the adjusted R^2 and predicted R^2 requires to be 0.20 away from each other and all of the analyzed parameters had these results. An equation in mathematics shows the connection between various causes and outcomes; (+) sign exhibits a synergistic effect, whereas (−) sign exhibits an antagonistic effect. The values of the coefficient X_1, X_2 and X_3 indicate how these variables affect the associated responses.

3.3. Characterization of DUL-loaded elastosomes

3.3.1. Effect of formulation variables on the entrapment efficiency percentage (E.E.%) of the developed DUL-loaded elastosomes

Significant barrier to effective drug delivery systems is the capacity of these vesicles to entrap high percentage of drug with minimum leakage (Abd-Elal et al., 2016). The E.E.% values of DUL within the developed elastosomal nanovesicles were listed in Table 3 and ranged from 70.3 ± 4.1% to 88.9 ± 1.8%. The effect of span®60: CH ratio (X_1), EA type (X_2) and EA amount (X_3) on E.E.% was statistically estimated by ANOVA and graphically displayed (Fig. 1A). The regression equation for E.E.% in terms of coded factors, was as following:

$$Y_1 = 79.325 + 2.35 \times {}_1 - 3.65 \times {}_2 - 2.675 \times {}_3 \quad (4)$$

The impact of span®60: CH ratio wasn't previously explored, where previous publications on elastosomes used fixed span® 60: CH ratios; 4:1 (Mosallam et al., 2021) and 5:1 (Aziz et al., 2018). In our study, varying the span®60: CH ratio (X_1) significantly ($p = 0.0072$) influenced the DUL E.E.%. Vesicles developed at a span®60: CH ratio of 5:1 (DUL-E5 - DUL-E8) revealed higher E.E.% compared to those developed at a span®60: CH ratio of 1:1 (Fig. 1A). This result could be explained in the light of the positive influence of span®60 on DUL E.E.%. The physicochemical properties of span®60; solid, saturated C_{18} alkyl chain with lipophilic properties (HLB value: 4.7) and high transition temperature (53 °C), enhance the encapsulation of more drug with minimum leakage (Tawfik et al., 2021; Zafar et al., 2022a). In a parallel line, previous study declared that the lower the HLB values of the vesicles' components, the more the drug entrapment within the hydrophobic core of the vesicular bilayers (Mosallam et al., 2021).

EA type revealed a significant ($P = 0.0014$) effect on the E.E.% of the developed DUL-loaded elastosomes. Brij S2 based vesicles exhibited higher E.E.% in comparison to cremophor RH 40 based vesicles. This finding could be correlated to the difference in the hydrophobicity of both EAs, where brij S2 (HLB value: 4) is more hydrophobic than cremophor RH 40 (HLB value: 16) (Aziz et al., 2018). As mentioned previously, brij S2 based vesicles being more lipophilic, can effectively entrap more lipophilic DUL within their hydrophobic bilayers (Abdelbary and Aburahma, 2015; Mosallam et al., 2021).

Increasing the EA amount considerably ($p = 0.0045$) reduced the E.E.% of the developed DUL-loaded elastosomes. This finding could be attributed to the leakage of DUL from the elastosomal vesicles via formation of pores within the vesicles' membranes. Moreover, this could be related to the solubilization or diffusion of DUL into the external medium on elevating the EA amount, resulting in significant lower drug E.E.%. Taking into consideration the fact that upon increasing the EA concentration till the critical micelle concentration is reached, drug solubilization takes place, inhibiting further drug entrapment (Fahmy et al., 2021).

3.3.2. Effect of formulation variables on the particle size (PS), polydispersity index (PDI), and zeta potential (ZP) of the developed DUL-loaded elastosomes

It is beneficial to develop vesicles with tiny PS to enhance their penetration through the membrane tissues. The PS values of the developed DUL-loaded elastosomes were listed in Table 3, ranged from 385 ± 21.5 nm to 751 ± 17.3 nm. The effect of span®60: CH ratio (X_1), EA type (X_2) and EA amount (X_3) on PS was assessed by ANOVA and graphically displayed (Fig. 1B). The regression equation for PS in terms of coded factors, was as following:

$$Y_2 = 547.625 + 155.625 \times {}_1 - 20.875 \times {}_2 - 21.375 \times {}_3 \quad (5)$$

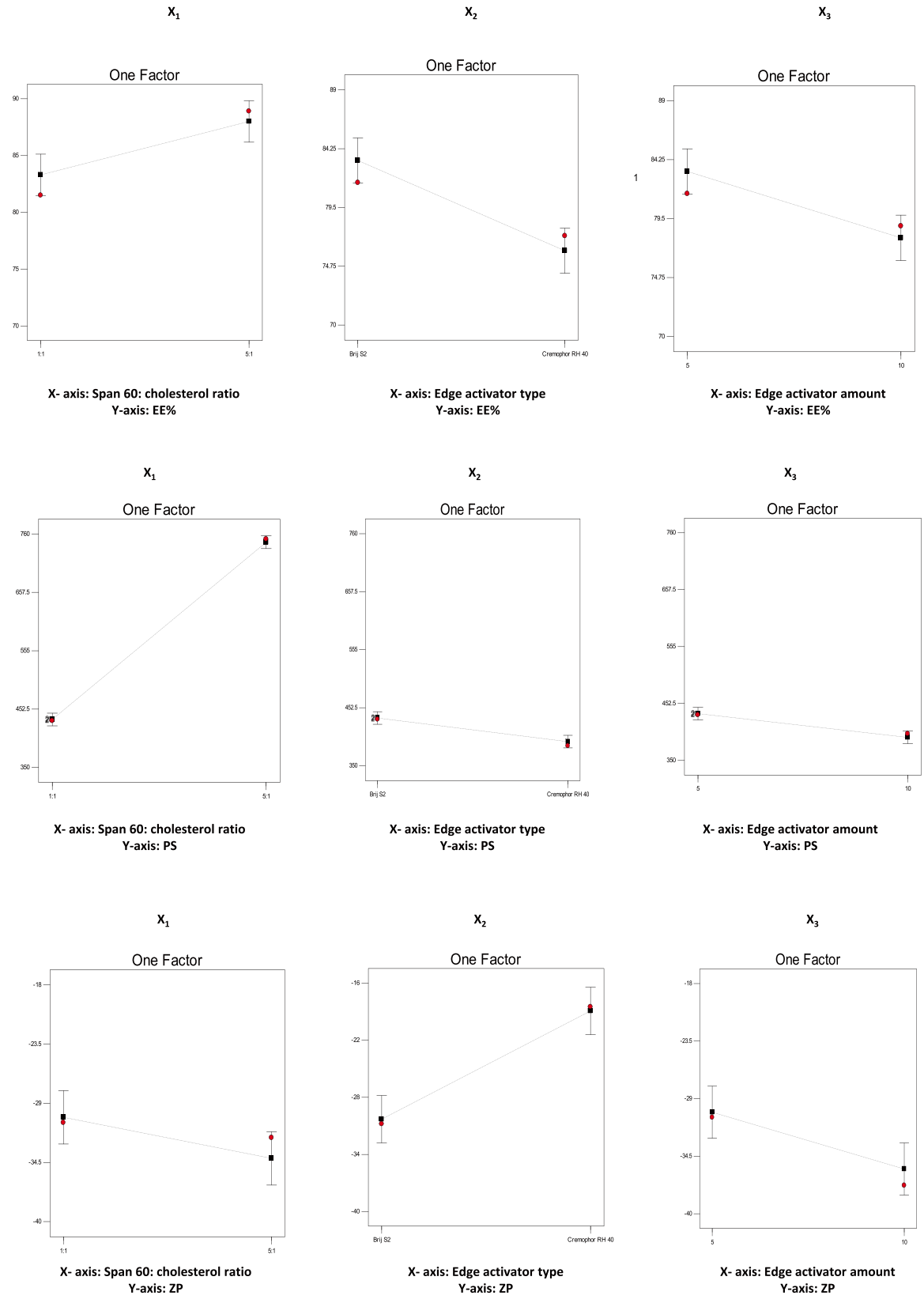

Fig. 1. A.: Effect of formulation variables on the entrapment efficiency percentage (E.E.%) of the developed DUL-loaded elastosomes.
B.: Effect of formulation variables on the particle size (PS) of the developed DUL-loaded elastosomes.
C.: Effect of formulation variables on the zeta potential (ZP) of the developed DUL-loaded elastosomes.
D.: Effect of formulation variables on the cumulative DUL released percentages after 0.5 h ($Q_{0.5h}$) from the developed DUL-loaded elastosomes.
E.: Effect of formulation variables on the cumulative DUL released percentages after 8 h (Q_{8h}) from the developed DUL-loaded elastosomes.

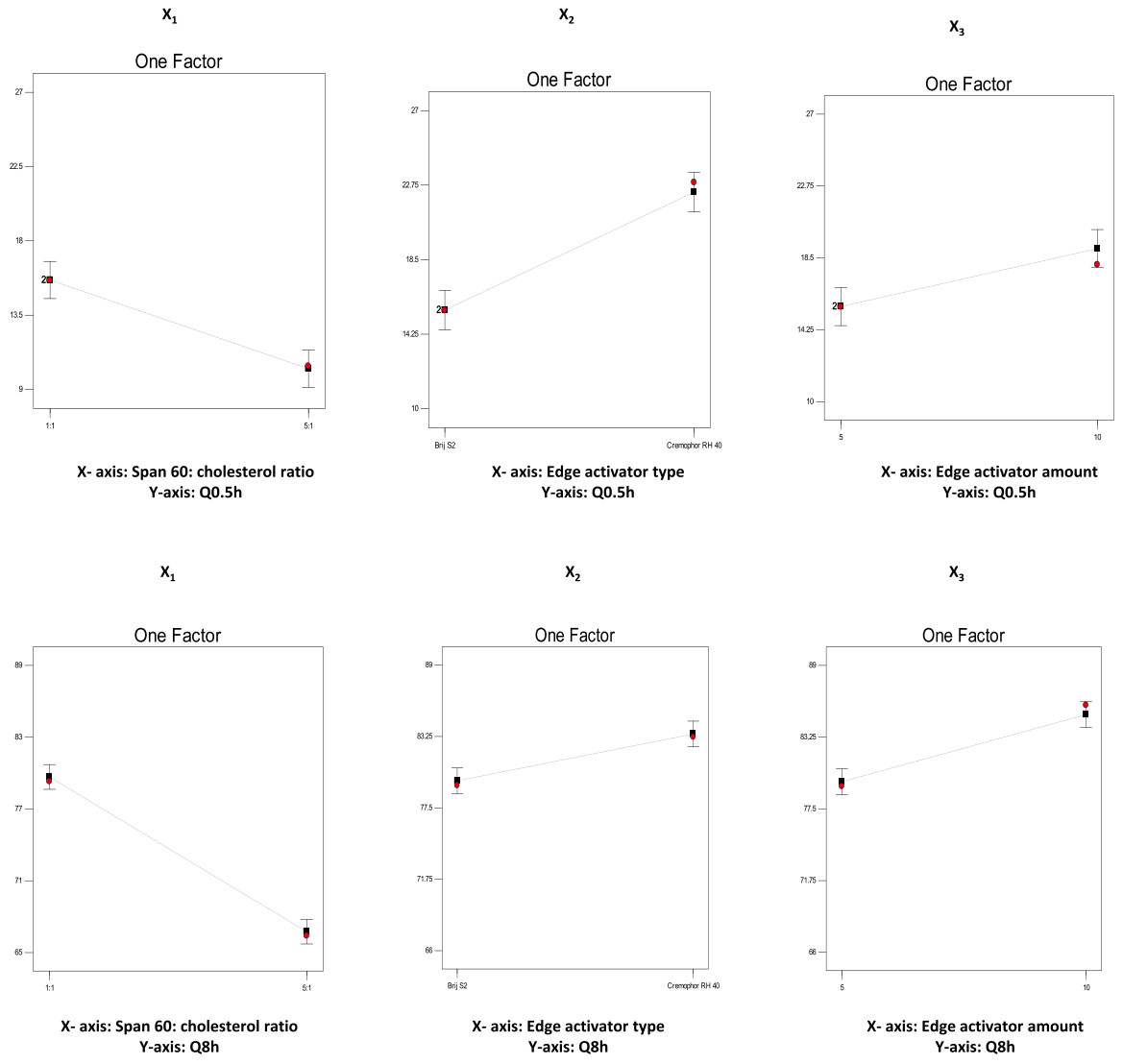

Fig. 1. (*continued*).

Span®60: CH ratio significantly ($p < 0.0001$) affected the PS of the developed DUL-loaded elastosomes, where elastosomes bearing a span®60: CH ratio of 5:1 (DUL-E5 - DUL-E8) showed greater PS compared to their corresponding ones bearing a span®60: CH ratio of 1:1. These findings are in a close agreement with those of E.E.%. The positive contribution of span®60 on the lipophilicity of the developed elastosomes, and hence the E.E.%, could be the reason for the larger PS.

Moreover, EA type had a significant ($p = 0.0018$) influence on the PS of the developed DUL-loaded elastosomes. Brij S2 based vesicles exhibited greater PS compared to their corresponding cremophor RH 40 based ones. Although it was expected that cremophor RH 40 based elastosomes reveal larger PS owing to their higher molecular weight. However, the current results are supported by the E.E.% findings, where brij S2 based vesicles showed higher E.E.%, in comparison to cremophor RH 40 based vesicles, due to its greater lipophilicity which enhanced greater DUL entrapment within the hydrophobic bilayers, and consequently greater PS.

Increasing the EA amount (X_3) significantly ($p = 0.00017$) reduced the PS of the developed DUL-loaded elastosomes. This results could be attributed to the decreased interfacial tension with increased EA amount, thus increased capability of emulsification and micelle formation, leading to reduced tendency towards aggregation (Basha et al., 2013; Fahmy et al., 2021). These findings were also in agreement with the E.E.% results, where the higher the E.E.%, the greater the PS.

The developed DUL-loaded elastosomes showed PDI values varying from 0.13 ± 0.04 (DUL-E4) to 0.61 ± 0.16 (DUL-E5), data not presented. The PDI values were directly correlated to the PS. Except for DUL-E5, all elastosomes revealed low PDI < 0.3, indicating the successful development of uniform elastosomal dispersions.

The stability of DUL-loaded elastosomes was determined through assessing the electric charges (ZP values) acquired by the vesicles. ZP values indicate how the systems are stable (Abd-Elal et al., 2016). In our study, high negative ZP values (ranging from −18.5 ± 1.4 to −39.4 ± 5.3 mV) were revealed, which were sufficient to prevent aggregation of vesicles during storage, as listed in Table 3. ZP variations are discussed in terms of their absolute values, to avoid confusion since all systems in our analysis had negative charges.

The impact of span®60: CH (X_1), EA type (X_2) and EA amount (X_3) on ZP values (mV) was estimated statistically and graphically displayed (Fig. 1C). The following equation showed the regression equation of ZP in term of coded factors as follow:

$$Y_3 = -29.2375 - 1.9125 \times {}_1 + 5.6875 \times {}_2 - 2.7125 \times {}_3 \quad (6)$$

Span®60: CH ratio (X_1) had a significant ($p = 0.0392$) impact on the ZP values of the developed DUL-loaded elastosomes. Vesicles developed at a high span®60 concentration (span®60: CH ratio of 5:1) revealed

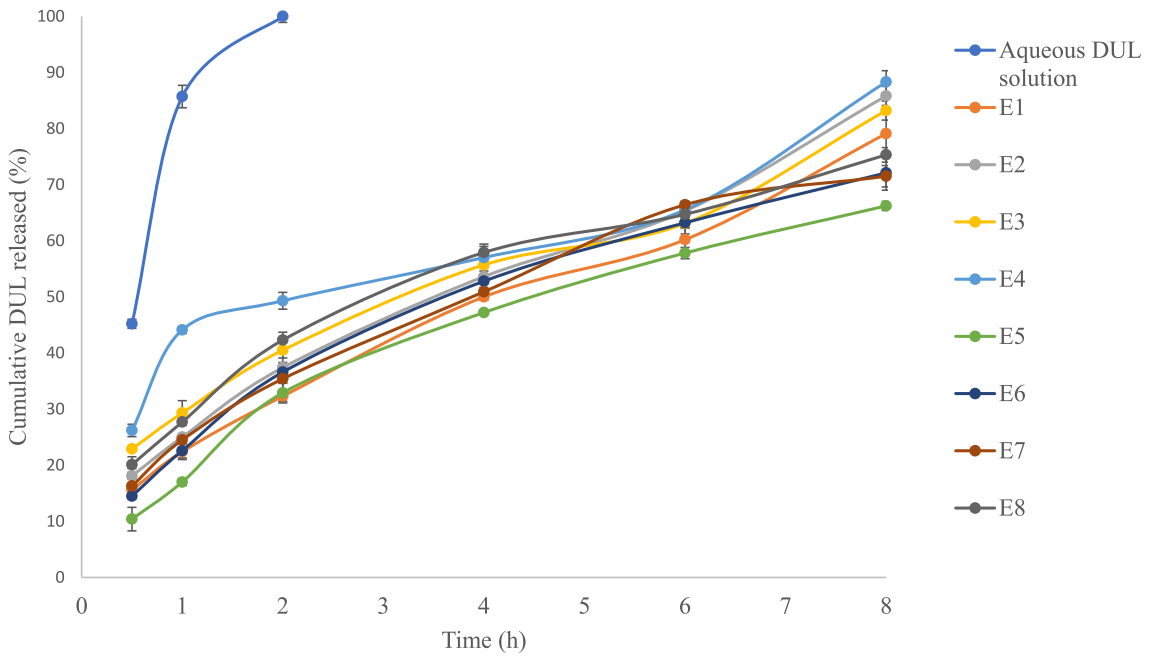

Fig. 2. In-vitro release profiles from the developed DUL-loaded elastosomes, in comparison to DUL aqueous solution.

higher absolute ZP values, in comparison to those developed at a low span®60 concentration (span® 60: CH ratio of 1:1). Increasing the span®60 concentration led to increase in charge, which in turn reduced the vesicles' aggregation and hence enhanced their stability (Khalil et al., 2013). Nonionic surfactants show an impact of the zeta potential in spite of being non ionized. This could be attributed to the molecular polarization or emulsifier adsorption on the acquired charges in water in the presence of SDC (an ionic compound). As a result, an electrical double layer might have been formed which reduced the aggregation of the vesicles. Similar observations were reported by Khalil et al. (2013) and Owodeha-Ashaka et al. (2021).

EA type (X_2) significantly ($p = 0.0009$) affected the ZP of the developed DUL-loaded elastosomes. Cremophor RH 40 based vesicles exhibited lower absolute ZP values in comparison to brij S2 based ones. This could be correlated to the difference in the hydrophilicities between brij S2 (HLB = 4) and cremophor RH 40 (HLB = 16). Owing to residing of cremophor RH 40 on the surface of the vesicular bilayer, and hence shielding of their surface charge, great lowering of the absolute ZP values was revealed (Aziz et al., 2018; Mosallam et al., 2021).

Moreover, boosting the EA amount (X_3) considerably ($P = 0.0128$) increased the ZP values of the developed DUL-loaded elastosomes. Such finding coincides with that obtained by Aziz et al. (2018) who found that 10 mg EA-based diacerein loaded elastosomes attained significantly higher ZP values, in comparison to 5 mg EA-based ones.

3.3.3. Effect of formulation variables on the cumulative DUL released percentages from the developed DUL-loaded elastosomes

The in-vitro release profiles from the developed DUL-loaded elastosomes as well as from DUL aqueous solution were illustrated in (Fig. 2). DUL released percentages from the aqueous solution were comparatively high, where almost all DUL was released within the first 2 h. Contrarily, the developed DUL-loaded elastosomes were capable of delaying the drug's release up to 8 h, where DUL released percentages after 0.5 h ($Q_{0.5h}$) ranged from 10.4 ± 1.8 (DUL-E5) to 26.2 ± 1.5 (DUL-E4) and after 8 h (Q_{8h}) ranged from 66.4 ± 0.8 (DUL-E5) to 88.7 ± 2 (DUL-E4). Biphasic release manner was attained from the developed elastosomes, with a rapid release phase, followed by a slower one. The fast partitioning of the surface adsorbed DUL into the release media, which is responsible for the burst effect and rapid beginning of action. Subsequently, slower sustained release phase was attained owing to the slow partitioning of the entrapped drug, which is responsible for maintaining the response over long period. The in-vitro release profile from equivalent DUL-E1 gel was conducted and revealed retarded release owing to the gel's viscosity, however it showed non-significant different $Q_{0.5h}$ and Q_{8h} ($p > 0.05$, from those obtained from DUL-E1 elastosomes.

The effect of span®60: CH (X_1), EA type (X_2) and EA amount (X_3) on the DUL released percentages after 0.5 h ($Q_{0.5h}$) and 8 h (Q_{8h}) were estimated statistically and graphically displayed in (Fig. 1D and 1E, respectively). The regression equations for $Q_{0.5h}$ and Q_{8h} in terms of coded factors, were as following:

$$Y_4 = 18.0125 - 2.6875 \times {}_1 + 3.3625 \times {}_2 + 1.7125 \times {}_3 \quad (7)$$

$$Y_5 = 77.7875 - 6.4625 \times {}_1 + 1.8875 \times {}_2 + 2.6875 \times {}_3 \quad (8)$$

Statistical analysis revealed that DUL released percentages after 0.5 h ($Q_{0.5h}$) and 8 h (Q_{8h}) were significantly ($p = 0.0007$, $p < 0.0001$, respectively) higher with elastosomes prepared at a span®60: CH ratio of 1:1, compared to those prepared at a span® 60: CH ratio of 5:1. These results can be explained in the light of E.E.% and PS results, where increasing span®60 revealed higher DUL entrapment as well as greater particle size, which were responsible for lowering the drug release rate owing to the greater mass transfer resistance (Tawfik et al., 2020). Comparable results were introduced by Fatouh et al. (2017) who emphasized the impact of entrapment on retarding the rate of drug release.

Moreover, EA type (X_2) also had significant ($p = 0.0003$, $p = 0.002$, respectively) effect on $Q_{0.5h}$ and Q_{8h}. Brij S2 based vesicles exhibited lower drug release percentages compared to cremophor RH 40 based vesicles. This could be related to the more hydrophobic nature of brij S2 as well as greater particle size, which decreased the drug release to the surrounding release media (Aziz et al., 2018). These results run with that published by Tawfik et al. (2018), they revealed the impact of vesicle's hydrophobicity on decreasing the drug diffusion into the release medium.

Furthermore, EA amount (X_3) had significant ($p = 0.004$, $p = 0.0005$, respectively) effects on DUL released percentages after 0.5 h and 8 h. Increasing the amount of EA resulted in more drug released percentages

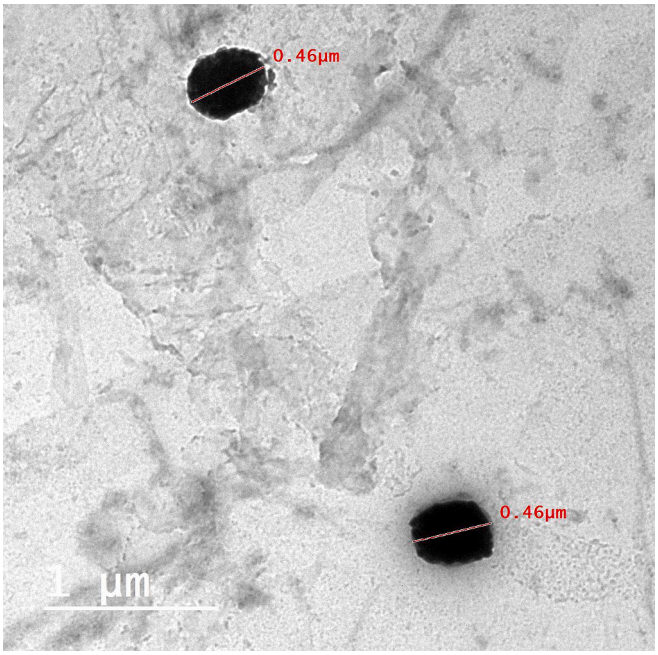

Fig. 3. Transmission electron micrograph of a representative DUL-loaded elastosomal system (DUL-E1).

from the developed vesicles. These findings were in close agreement with those of PS. The smaller PS of the developed vesicles exhibited more surface area available for release media and hence higher drug released percentages were attained (Abd-Elal et al., 2016). Previous studies reported the positive impact of PS on retarding the drug release from lipophilic vesicular systems (Tawfik et al., 2018).

3.4. Selection of the optimum DUL-loaded elastosomes

Based on the results obtained from the eight developed DUL-loaded elastosomes; Design Expert® software assessed the desirability in order to choose the optimum system with ideal physicochemical characteristics (AlAl-Mahallawi et al., 2014; Aziz et al., 2018). The desirability constraints of maximum E.E.%, ZP (absolute value), $Q_{0.5h}$ and Q_{8h} with minimum PS were achieved in DUL-E1 elastosomes, with high desirability value of 0.834. DUL-E1, comprised of CH, span®60 (at a span®60: CH ratio of 1:1), and EA (brij S2; 5 mg), showed E.E.% of 81.5 ± 3.2%, PS of 432 ± 13.2 nm, ZP of −30.8 ± 3.3 mV, $Q_{0.5h}$ and Q_{8h} values of 15.6 ± 0.9% and 79.3 ± 3.8%, respectively.

3.5. Characterization of the optimum DUL-loaded elastosomes

3.5.1. Morphological examination

TEM images of the optimum DUL-loaded elastosomes (DUL-E1) revealed well identified, spherical, non-aggregating vesicles with smooth surfaces (Fig. 3). In addition to that, the diameter of the optimum DUL-E1 obtained from TEM image was in good agreement with that observed by Malvern Zetasizer.

3.5.2. Deformability index (DI)

Deformability index values explain how the vesicular systems can squeeze themselves through membrane pores smaller than their own size without rupture (Kakkar and Kaur, 2011; Mosallam et al., 2021). High values of DI were obtained from the optimum DUL-E1 elastosomes (14.23 ± 1.43 g), which were significantly ($p < 0.05$) higher than their corresponding values obtained from DUL-loaded bilosomes (6.75 ± 0.5 g). This could be correlated to the presence of EA (brij S2) which increase the fluidity of the vesicles and, consequently form more elastic vesicles than their corresponding DUL-loaded bilosomes (Bsieso et al., 2015; Mosallam et al., 2021).

3.5.3. Differential scanning calorimetry (DSC) Studies

Fig. 4 illustrated the DSC thermograms of pure drug, each component

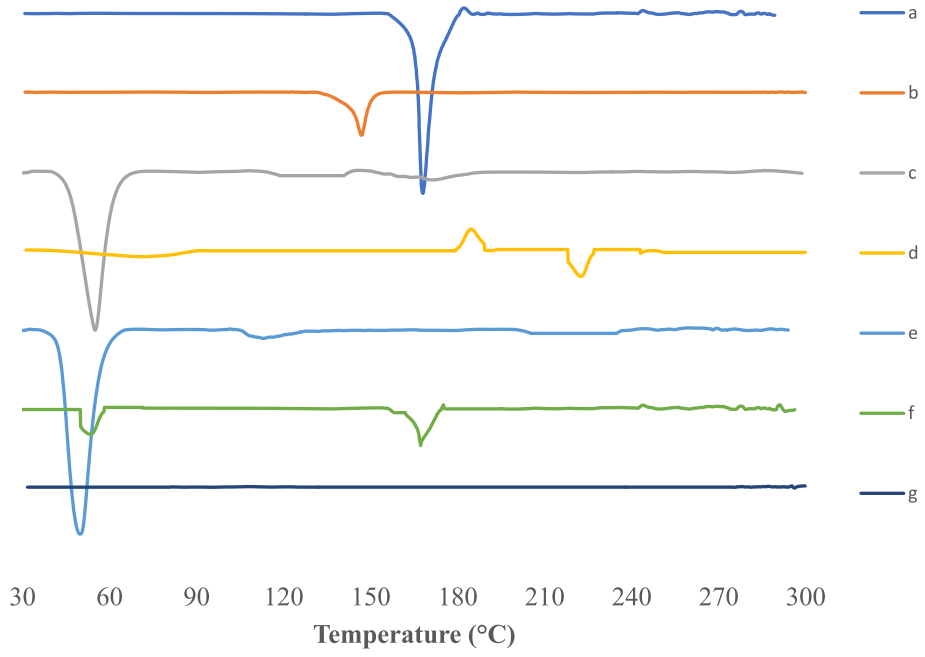

Fig. 4. DSC thermograms of DUL (a), cholesterol: CH (b), Span® 60 (c), sodium deoxycholate: SDC (d), brij S2 (e), physical mixture of DUL with elastosomal components (f) and DUL-E1 lyophilized elastosomes (g).

Table 4
Effect of storage on the characterization of the optimum DUL*-loaded elastosomes (DUL-E1).

Storage conditions	E.E.* (%)	PS* (nm)	PDI*	ZP* (mV)
DUL-E1 at 25 °C (freshly prepared)	81.5 ± 3.2	432 ± 13.2	0.24 ± 0.02	−30.8 ± 3.3
DUL-E1 at 25 °C (after 3 months)	78.9 ± 2.5	443 ± 9.7	0.33 ± 0.06	−28.4 ± 2.3
DUL-E1 at 4 °C (after 3 months)	79.6 ± 1.6	438 ± 20.4	0.3 ± 0.04	−30 ± 1.2

DUL: Duloxetine hydrochloride; E.E.: entrapment efficiency; PS: particle size; PDI: polydispersity index; ZP: zeta potential.

of the optimum developed elastosomes, physical mixture of all components along with the drug and finally DUL-E1 (optimum lyophilized elastosomes). Analysis of the thermal behavior of the drug was conducted throughout the optimum system, to shed light on any potential interaction and to determine the crystalline or amorphous nature of the drug. Pure DUL thermogram displayed sharp endothermic peak at 167.87 °C, related to its crystalline state (Elsenosy et al., 2020; Pandya et al., 2015). The decomposition of cholesterol revealed a sharp endothermic peak around 147 °C (Abd-Elal et al., 2016; Al-Mahallawi et al., 2015). In accordance with their respective melting points, span®60 and brij S2 had endothermic peaks at 55.01 and 49.88 °C, respectively (Aziz et al., 2018). While, SDC showed exothermic peak around 190 °C (Ahmed et al., 2020). The drug's characteristic endothermic peak was seen in the physical mixture's thermogram. However, it was absent in the lyophilized DUL-E1's thermogram. This declared that DUL was effectively embedded within the vesicular bilayers, in its amorphous form.

3.5.4. *Effect of short-term storage after 3 months*

In order to develop successful nanovesicular drug delivery systems, their stability is a crucial factor (Abd El-Alim et al., 2019). As shown in (Table 4), non-significant ($p > 0.05$) differences were observed in E.E.%, PS, PDI and ZP values of the freshly prepared optimum DUL-E1 elastosomes, in comparison to their corresponding stored ones at 4 ± 2 °C and 25 ± 2 °C after 3 months, respectively. Non-significant change in E.E.% proved the successful entrapment of drug within the elastosomal vesicles. The inclusion of the negatively charged SDC could be the reason for the non-significant changes in PS, PDI and ZP (Ahmed et al., 2020). Moreover, no physical nor chemical changes were detected. These findings confirmed the reasonable stability of DUL-E1 elastosomes.

3.5.5. *In-vitro characterization of DUL-E1 gel*

3.5.5.1. Determination of pH. The pH of DUL-E1 gel was 5.32 ± 0.09 which is considered to be safe and is believed to cause no irritation after application (Fahmy et al., 2018).

3.5.5.2. Determination of the rheological constants. DUL-E1 gel revealed shear thinning flow, owing to the decrease in viscosity upon elevated shear rate. Flow index value (n) of DUL-E1 gel was found to be 0.4129, which is far smaller than one. Consequently, DUL-E1 gel revealed shear thinning behavior and non-Newtonian flow (Fahmy et al., 2018).

3.5.6. *In-vivo DUL pharmacokinetic studies in rats*

The DUL plasma concentration-time profiles following the intranasal

Table 5
The estimated pharmacokinetic parameters and relative bioavailability (%) of Duloxetine HCl following the intranasal and the transdermal application of DUL-E1 (test treatments) versus the oral administration of DUL aqueous solution (reference treatment) in rats (mean ± s.d., $n = 6$).

Pharmacokinetic parameters	Intranasal DUL-E1	Transdermal DUL-E1	Oral DUL aqueous solution
C_{max} (ng/mL)	251 ± 18.6	248 ± 15.9	135 ± 8.6
T_{max} (h)	2 (2–2)	4 (2–4)	2 (2–2)
Tel (h)	20.4 ± 0.6	22.3 ± 0.8	12 ± 0.4
$MRT_{0-\infty}$ (h)	29.7 (29.2–30.4)	32.7 (31.9–33.5)	18 (17–18.7)
AUC_{0-72} (ng.h/mL)	6273 ± 267	6842.5 ± 230	2416.3 ± 62
$AUC_{0-\infty}$ (ng.h/mL)	6884.5 ± 275	7703.7 ± 239	2456.3 ± 68
Relative Bioavailability based on $AUC_{0-\infty}$ (%)	280.28	313.63	–

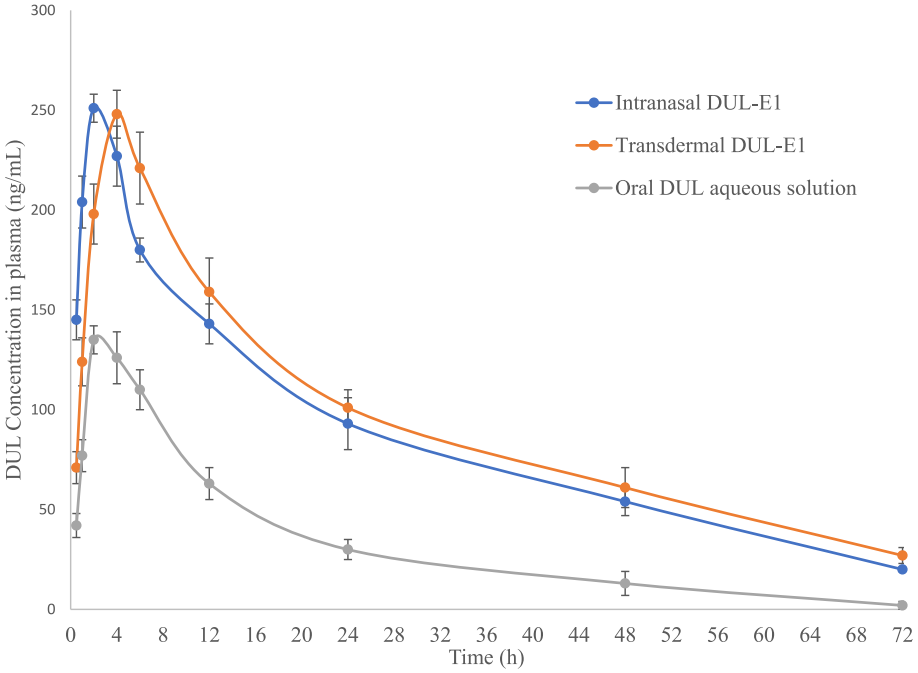

Fig. 5. Duloxetine HCl plasma concentration-time profiles following the intranasal and transdermal application of DUL-E1 (test treatments) versus the oral administration of DUL aqueous solution (reference treatment) in rats (mean ± s.d., n = 6).

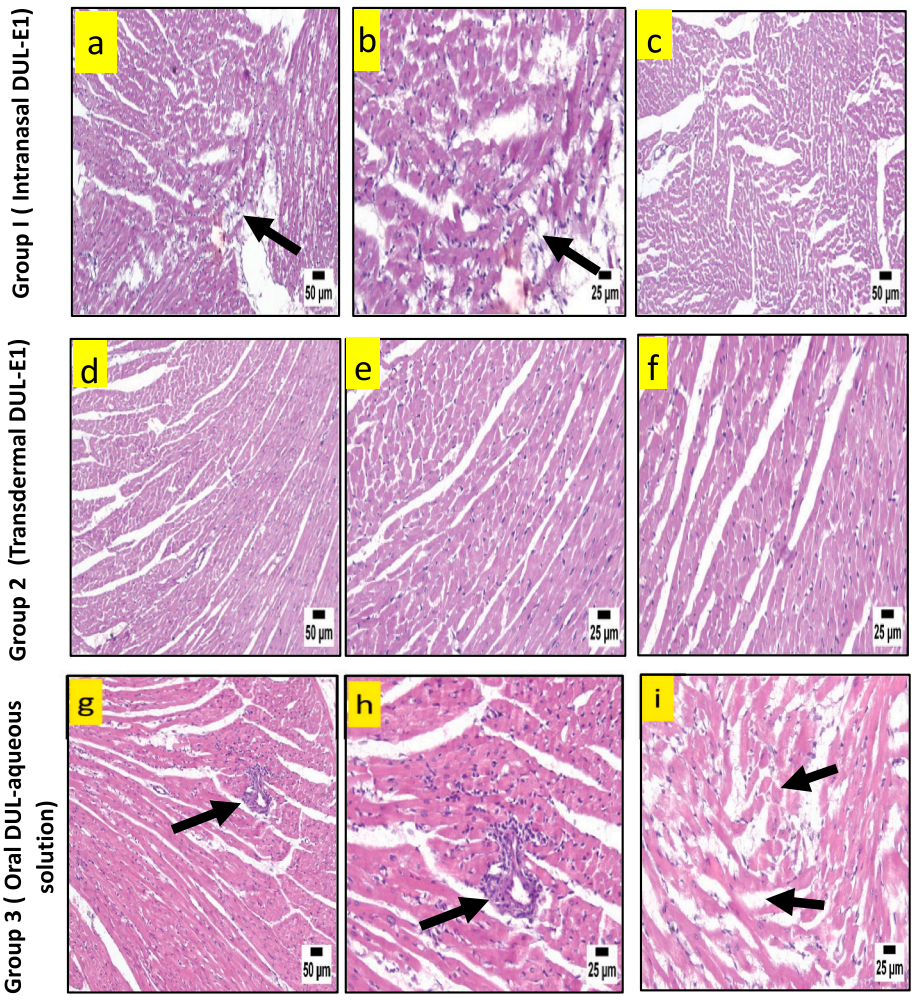

Fig. 6. A.: Histopathological view of heart after H&E staining in rats; group 1 (intranasal DUL-E1), group 2 (transdermal DUL-E1), and group 3 (oral DUL aqueous solution).
B.: Histopathological view of liver after H&E staining in rats; group 1 (intranasal DUL-E1), group 2 (transdermal DUL-E1), and group 3 (oral DUL aqueous solution).
C.: Histopathological view of brain after H&E staining in rats; group 1 (intranasal DUL-E1), group 2 (transdermal DUL-E1), and group 3 (oral DUL aqueous solution).

and the transdermal application of DUL-E1, respectively (test treatments) versus the oral administration of DUL aqueous solution (reference treatment) are shown in Fig. 5. DUL pharmacokinetic parameters were derived and tabulated, for comparative purpose (Table 5).

Interestingly, the C_{max} of both test treatments were significantly ($P < 0.01$) different from the C_{max} of the reference treatment. Oral DUL aqueous solution attained significantly low C_{max} (135 ng/mL), at median T_{max} of 2 h. Following the intranasal application of DUL-E1, maximum DUL concentration (251 ± 18.6 ng/mL) was reached at a median T_{max} (2 h) similar to the T_{max} of the reference treatment. This rapidly achieved T_{max} value could emphasize the fast drug absorption via the intranasal route (Abd-Elal et al., 2016; Elsenosy et al., 2020). However, upon the application of DUL-E1 transdermally, significant ($P < 0.01$) high C_{max} value (248 ± 15.9 ng/mL) was revealed at a significant delayed median T_{max} (4 h). The observed delayed T_{max} might be a result of the barrier effect of the skin on drug penetration (Tawfik et al., 2020). Modified release of DUL-E1 via the intranasal route could be proved by the significantly ($P < 0.01$) prolonged elimination half-life (from 12 h to 20.4 h) and MRT $_{(0-\infty)}$ (from 18 h to 29.7 h). This finding might be attributed to the low clearance of DUL-E1 gel, and subsequently prolonged mucociliary transit time (El Taweel et al., 2021; Elsenosy et al., 2020). In a parallel line, transdermal DUL-E1 attained significantly ($P < 0.01$) delayed median T_{max} (from 2 h to 4 h), beside the significant ($P < 0.01$) elongation in the elimination half-life (from 12 h to 22.3 h) and in the MRT $_{(0-\infty)}$ (from 18 h to 32.7 h). This could be explained in the light of the prolonged circulation interval of the vesicles via the transdermal route. Moreover, the skin might act as a reservoir for DUL-E1, thus maintaining effective DUL concentration over an extended period (Fahmy et al., 2018).

Compared to oral DUL aqueous solution, significant ($P < 0.01$) enhancement of the DUL's bioavailability was noticed following the application of both test treatments. After intranasal and transdermal application of DUL-E1, the calculated relative bioavailabilities were 280.30% and 313.6%, respectively [upon comparing the AUC $_{(0-\infty)}$ values of 6884.5 ng•h/mL and 7703.7 ng•h/mL, respectively (test treatments) versus 2456.3 ng•h/mL (reference treatment)].

The enhanced bioavailability of DUL could be credited to various factors including, (i) the tiny particle size of the developed nanovesicles (432 ± 13.2 nm) (Hassan et al., 2022), (ii) the elevated surface area: volume ratio of the prepared vesicles, which enhanced the intimate contact and residence time of DUL-E1 with the nasal mucosa (El Taweel et al., 2021; Elsenosy et al., 2020) and the skin (Tawfik et al., 2021), (iii) the high elasticity (D1; 14.23 ± 1.43 g) of the elastosomes which facilitated their penetration (Aziz et al., 2018; Mosallam et al., 2021) owing to the combined effects of surfactants (span®60, SDC) and EA, (iv) the small molecular weight (330 g/mol) and great lipophilicity of DUL (log

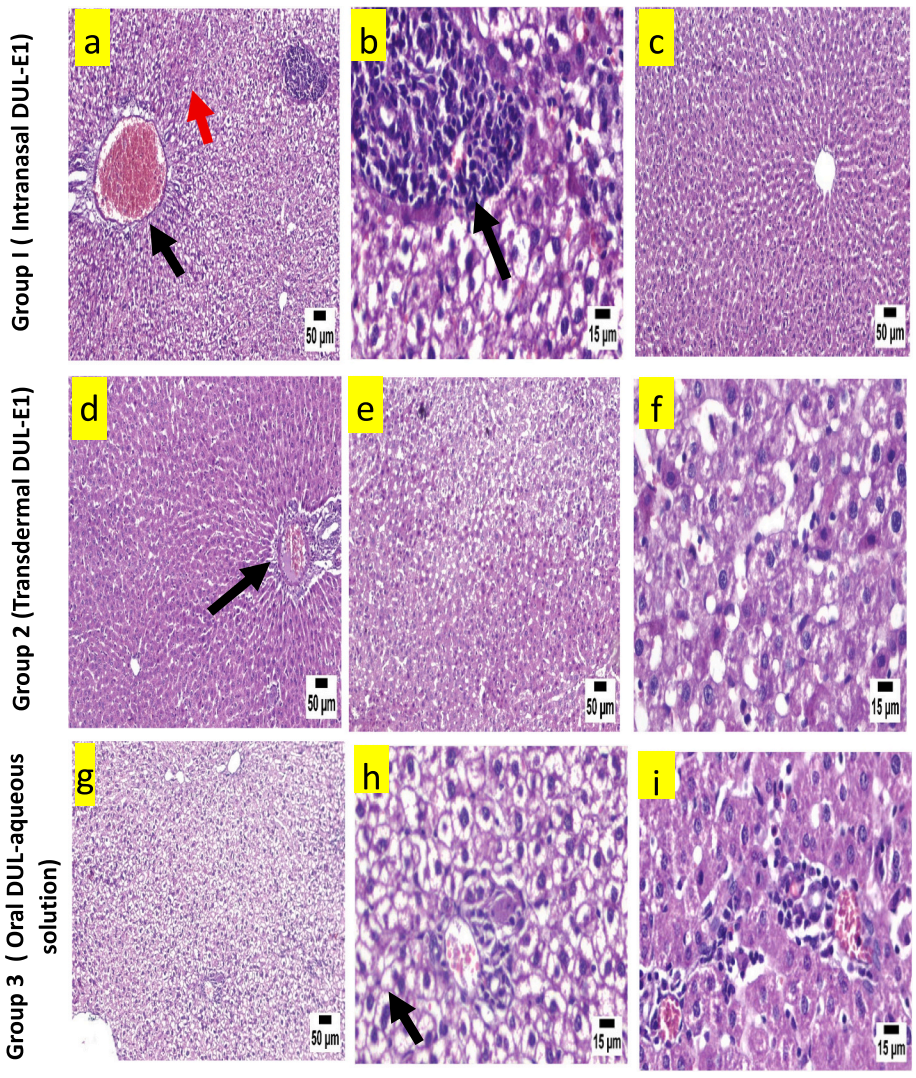

Fig. 6. (*continued*).

$P = 4.2$) (Elsenosy et al., 2020), which made DUL a good candidate for intranasal and transdermal routes, as well as for crossing the BBB, and (v) the avoidance of the extensive acidic degradation in the gastrointestinal tract as well as the enzymatic and liver metabolism (Elsenosy et al., 2020; Hassan et al., 2022; Tawfik et al., 2021). It is worth mentioning that the intranasal route has the privilege of bypassing the BBB and transferring the drug directly to the brain via the olfactory pathway, beside the systemic absorption (El Taweel et al., 2021; Elsenosy et al., 2020; Yasir et al., 2022a).

3.5.7. *In-vivo DUL histopathological studies*

Histopathology of heart in group 1 revealed mild edema with few mononuclear inflammatory cells infiltrating the myocardium (Fig. 6a & b), meanwhile an apparently normal heart structure was observed in the majority of the examined sections (Fig. 6c), following the intranasal application of DUL-E1. Apparently normal myocardium was revealed upon the transdermal application of DUL-E1 (group 2) (Fig. 6d, e & f). However, oral DUL aqueous solution declared marked histopathological changes, where intense perivascular lymphocytic infiltration, inflammatory edema (Fig. 6g &h), and necrosed and hyalinized myocardial fibers (Fig. 6i) were observed.

The examination of liver following the intranasal application of DUL-E1 revealed diffuse hepatocellular vacuolation in the hepatic parenchyma characterized by existence of clear cytoplasmic vacuoles in hepatocytes, with centrally located nuclei and congested blood vessel (Fig. 6a & b). Some of the examined sections showed portal congestion and infiltration with mononuclear inflammatory cells (Fig. 6a). On the other hand, others showed apparently normal liver structure (Fig. 6c). Group 2 showed mild portal infiltration with mononuclear inflammatory cells and apparently normal hepatocytes (Fig. 6d), following the transdermal application of DUL-E1. While some other sections exhibited hepatocellular degeneration and necrosis (Fig. 6e & f). Severe diffuse hepatocellular vacuolation, portal infiltration with mild mononuclear inflammatory cells infiltration were the main histological features of group 3 (Fig. 6g, h & i).

Microscopic examination of brain sections of group 1 revealed few congested blood vessels in the cerebral cortex associated with mild neuronal edema and few degenerated neurons (Fig. 6a). Apparently normal different regions of hippocampus (normal CA1-CA4 regions of the hippocampus (Fig. 6b-f) and normal DG region of the hippocampus (Fig. 6f)) were detected. Apparently normal cerebral cortex was detected in group 2 (Fig. 6g). Similarly, the hippocampus revealed normal neurons in different regions; CA1-CA4 (Fig. 6h-k), and DG (Fig. 6l). Neuronal degeneration and neuronophagia with diffuse gliosis were observed in group 3, following the administration of DUL solution orally (Fig. 6m). No abnormalities were determined in the neurons of the hippocampus (normal CA1-CA4 region of the hippocampus (Fig. 6n-q) and normal DG region of the hippocampus (Fig. 6r)).

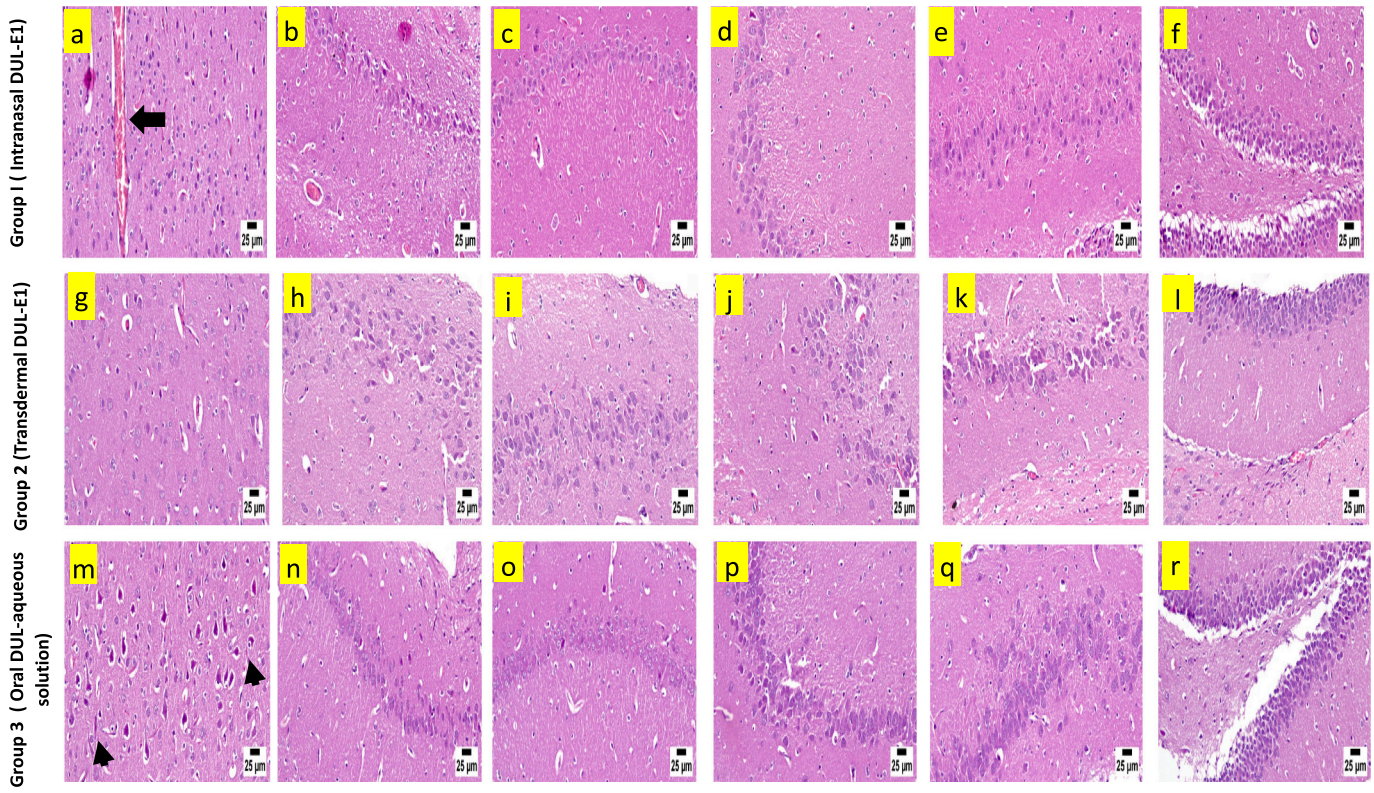

Fig. 6. (*continued*).

The obtained results emphasized that DUL-E1 was more preferential and showed higher safety following its intranasal as well as transdermal application, than oral DUL aqueous solution. However, in the light of the histopathological safety assessment results; the transdermal route declared better results in comparison to the intranasal one. The detected side effects that appeared on the investigated organs (heart, liver, and brain) following the administration of DUL aqueous solution could be correlated to ADME via the oral route. So, attempts have been adopted to deliver DUL via other various routes to avoid the hepatic metabolism and improve the bioavailability (El Sharawy et al., 2017; Khatoon et al., 2019; Salem et al., 2022). The histopathological results are in a parallel in with DUL in-vivo pharmacokinetic studies.

4. Conclusion

In our work, DUL-loaded elastosomes (ultra-elastic nanovesicles) were successfully developed with high drug loading in nano-sized range, via thin film hydration method. The optimimum DUL-loaded elastosomes (DUL-E1) showed the highest desirability value (0.834) with respect to maximum E.E.%, ZP (absolute value), $Q_{0.5h}$ and Q_{8h} along with minimum PS. Compared to oral DUL aqueous solution, the pharmacokinetics in rats emphasized the potential of DUL-E1 elastosomes, via intranasal as well as transdermal route owing to its ultra-elastic properties. DUL-E1 succeeded to improve the bioavailability of the drug and modify its release rate, to initiate as well as maintain DUL response for an extended period. Moreover, the safety of DUL-E1 after intranasal and transdermal application was confirmed by in-vivo histopathological studies. Finally, DUL-loaded elastosomes could constitute an advance in depression management by increasing the bioavailability of duloxetine hydrochloride via various routes of administration with great safety.

Funding

This research did not receive any specific grant from funding agencies in the public, commercial, or not-for-profit sectors.

CRediT authorship contribution statement

Radwa M.A. Abd-Elal: Writing – original draft, Writing – review & editing, Data curation, Supervision, Visualization, Conceptualization, Investigation, Validation. **Aya M. Essawy:** Conceptualization, Methodology, Resources. **Maha A. Salem:** Conceptualization, Methodology, Resources. **Mahitab Elsayed:** Conceptualization, Methodology, Resources. **Mona G. Khalil:** Conceptualization, Methodology, Resources. **Eman Abdelhakeem:** Writing – original draft, Data curation, Visualization, Investigation, Validation. **Nouran A. Ali:** Writing – review & editing, Data curation, Visualization, Conceptualization. **Mai Ahmed Tawfik:** Writing – review & editing, Data curation, Supervision, Visualization, Conceptualization, Investigation, Validation.

Declaration of Competing Interest

The authors have no relevant financial or non-financial interests to disclose.

Data availability

Data will be made available on request.

References

Abd El-Alim, S.H., Kassem, A.A., Basha, M., Salama, A., 2019. Comparative study of liposomes, ethosomes and transfersomes as carriers for enhancing the transdermal delivery of diflunisal: in vitro and in vivo evaluation. Int. J. Pharmaceut. 30 (563), 293–303. https://doi.org/10.1016/j.ijpharm.2019. 04.001.

Abd-Elal, R.M.A., Shamma, R.N., Rashed, H.M., Bendas, E.R., 2016. Trans-nasal zolmitriptan novasomes: in-vitro preparation, optimization and in-vivo evaluation of brain targeting efficiency. Drug Deliv. 23 (9), 3374–3386. https://doi.org/10.1080/10717544.2016.1183721.

Abd-Elal, R.M.A., Elosaily, G.H., Gad, S., Khafagy, E.S., Mostafa, Y., 2020. Full factorial design, optimization, in vitro and ex vivo studies of ocular timolol-loaded

microsponges. J. Pharm. Innov. 15, 651–663. https://doi.org/10.1007/s12247-019-09418-z.
Abdelbary, G.A., Aburahma, M.H., 2015. Oro-dental mucoadhesive proniosomal gel formulation loaded with lornoxicam for management of dental pain. J. Liposome Res. 25 (2), 107–121. https://doi.org/10.3109/08982104.2014.941861.
Ahmed, S., Kassem, M.A., Sayed, S., 2020. Bilosomes as promising nanovesicular carriers for improved transdermal delivery: construction, in vitro optimization, ex vivo permeation and in vivo evaluation. Int. J. Nanomedicine 8 (15), 9783–9798. https://doi.org/10.2147/IJN.S278688.
Ali, A.A., Hassan, A.H., Eissa, E.M., Aboud, H.M., 2021. Response surface optimization of ultra-elastic nanovesicles loaded with deflazacort tailored for transdermal delivery: accentuated bioavailability and anti-inflammatory efficacy. Int. J. Nanomedicine 16, 591–607. https://doi.org/10.2147/IJN.S276330.
Al-Mahallawi, A.M., Khowessah, O.M., Shoukri, R.A., 2014. Nano-transfersomal ciprofloxacin loaded vesicles for non-invasive trans-tympanic ototopical delivery: in-vitro optimization, ex-vivo permeation studies, and in-vivo assessment. Int. J. Pharmaceut. 472 (1–2), 304–314. https://doi.org/10.1016/j.ijpharm.2014.06.041, 10.
Al-Mahallawi, A.M., Abdelbary, A.A., Aburahma, M.H., 2015. Investigating the potential of employing bilosomes as a novel vesicular carrier for transdermal delivery of tenoxicam. Int. J. Pharmaceut. 485 (1–2), 329–340. https://doi.org/10.1016/j.ijpharm.2015.03.033, 15.
Aziz, D.E., Abdelbary, A.A., Elassasy, A.I., 2018. Fabrication of novel elastosomes for boosting the transdermal delivery of diacerein: statistical optimization, ex-vivo permeation, in-vivo skin deposition and pharmacokinetic assessment compared to oral formulation. Drug Deliv. 25 (1), 815–826. https://doi.org/10.1080/10717544.2018.1451572.
Basha, M., Abd El-Alim, S.H., Shamma, R.N., Awad, G.E., 2013. Design and optimization of surfactant-based nanovesicles for ocular delivery of Clotrimazole. J. Liposome Res. 23 (3), 203–210. https://doi.org/10.3109/08982104.2013.788025.
Bsieso, E.A., Nasr, M., Moftah, N.H., Sammour, O.A., Abd El Gawad, N.A., 2015. Could nanovesicles containing a penetration enhancer clinically improve the therapeutic outcome in skin fungal diseases? Nanomedicine (London) 10 (13), 2017–2031. https://doi.org/10.2217/nnm.15.49.
Dai, Y., Zhou, R., Liu, L., Lu, Y., Qi, J., Wu, W., 2013. Liposomes containing bile salts as novel ocular delivery systems for tacrolimus (FK506): in vitro characterization and improved corneal permeation. Int. J. Nanomedicine 8, 1921–1933. https://doi.org/10.2147/IJN.S44487.
Desai, S., Doke, A., Disouza, J.I., Athawale, R., 2011. Development and evaluation of antifungal topical niosomal gel formulation. Int J Pharm Pharm Sci 3, 224–231.
El Sharawy, A.M., Shukr, M.H., Elshafeey, A.H., 2017. Formulation and optimization of duloxetine hydrochloride buccal films: in vitro and in vivo evaluation. Drug Deliv. 24 (1), 1762–1769. https://doi.org/10.1080/10717544.2017.140221634.
El Taweel, M.M., Aboul-Einien, M.H., Kassem, M.A., Elkasabgy, N.A., 2021. Intranasal zolmitriptan-loaded bilosomes with extended nasal mucociliary transit time for direct nose to brain delivery. Pharmaceutics. 13 (11), 1828. https://doi.org/10.3390/pharmaceutics13111828, 1.
El Zaafarany, G.M., Awad, G.A., Holayel, S.M., Mortada, N.D., 2010. Role of edge activators and surface charge in developing ultradeformable vesicles with enhanced skin delivery. Int. J. Pharmaceut. 397, 164–172. https://doi.org/10.1016/j.ijpharm.2010.06.034.
Elsenosy, F.M., Abdelbary, G.A., Elshafeey, A.H., Elsayed, I., Fares, A.R., 2020. Brain targeting of duloxetine HCL via intranasal delivery of loaded cubosomal gel: in vitro characterization, ex vivo permeation, and in vivo biodistribution studies. Int. J. Nanomedicine 30 (15), 9517–9537. https://doi.org/10.2147/IJN.S277352.
Fahmy, A.M., El-Setouhy, D.A., Ibrahim, A.B., Habib, B.A., Tayel, S.A., Bayoumi, N.A., 2018. Penetration enhancer-containing spanlastics (PECSs) for transdermal delivery of haloperidol: in vitro characterization, ex vivo permeation and in vivo biodistribution studies. Drug Deliv. 25 (1), 12–22. https://doi.org/10.1080/10717544.2017.1410262.
Fahmy, A.M., Hassan, M., El-Setouhy, D.A., Tayel, S.A., Al-Mahallawi, A.M., 2021. Statistical optimization of hyaluronic acid enriched ultradeformable elastosomes for ocular delivery of voriconazole via Box-Behnken design: in vitro characterization and in vivo evaluation. Drug Deliv. 28 (1), 77–86. https://doi.org/10.1080/10717544.2020.1858997.
Fatouh, A.M., Elshafeey, A.H., Abdelbary, A., 2017. Intranasal agomelatine solid lipid nanoparticles to enhance brain delivery: formulation, optimization and in vivo pharmacokinetics. Drug Des. Devel. Ther. 19 (11), 1815–1825. https://doi.org/10.2147/DDDT.S102500.
Gupta, P.N., Mishra, V., Rawat, A., Dubey, P., Mahor, S., Jain, S., Chatterji, D.P., Vyas, S.P., 2005. Non-invasive vaccine delivery in transfersomes, niosomes and liposomes: a comparative study. Int. J. Pharmaceut. 293, 73–82. https://doi.org/10.1016/j.ijpharm.2004.12.022.
Hassan, D.H., Shohdy, J.N., El-Setouhy, D.A., El-Nabarawi, M., Naguib, M.J., 2022. Compritol-based nanostrucutured lipid carriers (NLCs) for augmentation of zolmitriptan bioavailability via the transdermal route: in vitro optimization, ex vivo permeation, in vivo pharmacokinetic study. Pharmaceutics 14 (7), 1484. https://doi.org/10.3390/pharmaceutics14071484, 18.
Kakkar, S., Kaur, I.P., 2011. Spanlastics- a novel nanovesicular carrier system for ocular delivery. Int. J. Pharmaceut. 413 (1–2), 202–210. https://doi.org/10.1016/j.ijpharm.2011.04.027.
Khalil, R.M., Abd El-bary, A., Kassem, M.A., Ghorab, M.M., Basha, M., 2013. Influence of formulation parameters on the physicochemical properties of meloxicam-loaded solid lipid nanoparticles. Egypt. Pharm. J. 12, 63–72. https://doi.org/10.7123/01.EPJ.0000 428643. 74323.d9.
Khatoon, M., Sohail, M.F., Shahnaz, G., Ur Rehman, F., Fakhar-Ud-Din, Ur Rehman, A., Ullah, N., Amin, U., Khan, G.M., Shah, K.U., 2019. Development and evaluation of optimized thiolated chitosan proniosomal gel containing duloxetine for intranasal delivery. AAPS PharmSciTech 20 (7), 288. https://doi.org/10.1208/s12249-019-1484-y, 13.
Lei, W., Yu, C., Lin, H., Zhou, X., 2013. Development of tacrolimus-loaded transfersomes for deeper skin penetration enhancement and therapeutic effect improvement in vivo. AJPS. 8 (6), 336–345. https://doi.org/10.1016/j.ajps.2013.09.005.
Mosallam, S., Sheta, N.M., Elshafeey, A.H., Abdelbary, A.A., 2021. Fabrication of highly deformable bilosomes for enhancing the topical delivery of terconazole: in vitro characterization, microbiological evaluation, and in vivo skin deposition study. AAPS PharmSciTech 22 (2), 74. https://doi.org/10.1208/s12249-021-01924-z, 14.
Nemeroff, C.B., 2007. The burden of severe depression: a review of diagnostic challenges and treatment alternatives. J. Psychiatr. Res. 41 (3–4), 189–206. https://doi.org/10.1016/j.jpsychires. 2006.05.008.
Owodeha-Ashaka, K., Ilomuanya, M.O., Iyire, A., 2021. Evaluation of sonication on stability-indicating properties of optimized pilocarpine hydrochloride-loaded niosomes in ocular drug delivery. Prog. Biomater. 10 (3), 207–220. https://doi.org/10.1007/s40204-021-00164-5.
Pandya, P., Pandey, N., Singh, S.K., Kumar, M., 2015. Formulation and characterization of ternary complex of poorly soluble duloxetine hydrochloride. J. Appl. Pharm. Sci. 5 (6), 088–096. https://doi.org/10.7324/JAPS.2015.50615.
Peddapalli, H., Banala, N., Dudhipala, N., Chinnala, K.M., 2018. Transmucosal delivery of duloxetine hydrochloride for prolonged release: preparation, in vitro, ex vivo characteri-zation and in vitro-ex vivo correlation. Int. J. Pharmaceut. Sci. Nanotechnol. (IJPSN) 11 (5), 4249–4258. https://doi.org/10.37285/ijpsn.2018.11.5.5.
Rana, I., Khan, N., Ansari, M.M., Shah, F.A., Din, Fakhar Ud, Sarwar, S., Imran, M., Qureshi, O.S., Choi, H.-I., Lee, C.-H., Kim, J.-K., Zeb, A., 2020. Solid lipid nanoparticles-mediated enhanced antidepressant activity of duloxetine in lipopolysaccharide-induced depressive model. Colloids Surf. B: Biointerfaces 194, 111209. https://doi.org/10.1016/j.colsurfb.2020. 111209.
Reagan-Shaw, S., Nihal, M., Ahmad, N., 2008. Dose translation from animal to human studies revisited. FASEB J. 22 (3), 659–661. https://doi.org/10.1096/fj.07-9574lsf33.
Salem, H.F., Ali, A.A., Rabea, Y.K. Abo, El-Ela, F.I., Khallaf, R.A., 2022. Glycerosomal thermosensitive in situ gel of duloxetine HCl as a novel nanoplatform for rectal delivery: in vitro optimization and in vivo appraisal. Drug Deliv. Transl. Res. 12, 3083–3103. https://doi.org/10.1007/s13346-022-01172-z.
Setia, A., Kansal, S., Goyal, N., 2013. Development and optimization of enteric coated mucoadhesive microspheres of duloxetine hydrochloride using 3(2) full factorial design. Int. J. Pharmaceut. Investig. 3 (3), 141–150. https://doi.org/10.4103/2230-973X.119217.
Sharma, M., Kohli, S., Dinda, A., 2015. In-vitro and in-vivo evaluation of repaglinide loaded floating microspheres prepared from different viscosity grades of HPMC polymer. Saudi Pharm. J. 23 (6), 675–682. https://doi.org/10.1016/j.jsps.2015.02.013.
Tawfik, M.A., Tadros, M.I., Mohamed, M.I., 2018. Lipomers (lipid-polymer hybrid particles) of vardenafil hydrochloride: a promising dual platform for modifying the drug release rate and enhancing its oral bioavailability. AAPS PharmSciTech 19 (8), 3650–3660. https://doi.org/10.1208/s12249-018-1191-0.
Tawfik, M.A., Tadros, M.I., Mohamed, M.I., 2019. Polyamidoamine (PAMAM) dendrimers as potential release modulators and oral bioavailability enhancers of vardenafil hydrochloride. Pharm. Dev. Technol. 24 (3), 293–302. https://doi.org/10.1080/10837450.2018.1472611.
Tawfik, M.A., Tadros, M.I., Mohamed, M.I., El-Helaly, S.N., 2020. Low-frequency versus high-frequency ultrasound-mediated transdermal delivery of agomelatine-loaded invasomes: development, optimization and in-vivo pharmacokinetic assessment. Int. J. Nanomedicine 12 (15), 8893–8910. https://doi.org/10.2147/IJN.S283911.
Tawfik, M.A., Tadros, M.I., Mohamed, M.I., El-Helaly, S.N., 2021. Low-frequency sonophoresis as an active approach to potentiate the transdermal delivery of agomelatine-loaded novasomes: design, optimization, and pharmacokinetic profiling in rabbits. AAPS PharmSciTech 22 (8), 261. https://doi.org/10.1208/s12249-021-02147-y, 27.
Tawfik, M.A., Eltaweel, M.M., Fatouh, A.M., Shamsel-Din, H.A., Ibrahim, A.B., 2023. Brain targeting of zolmitriptan via transdermal terpesomes: statistical optimization and in vivo biodistribution study by 99mTc radiolabeling technique. Drug Deliv. Transl. Res. https://doi.org/10.1007/s13346-023-01373-0. Article No: 1373.
Van Den Bergh, B.A., Wertz, P.W., Junginger, H.E., Bouwstra, J.A., 2001. Elasticity of vesicles assessed by electron spin resonance, electron microscopy and extrusion measurements. Int. J. Pharmaceut. 217, 13–24. https://doi.org/10.1016/s0378-5173(01)0057-2.
Vishwakarma, S.K., Sharmila, P., Bardia, A., Chandrakala, L., Raju, N., Sravani, G., Sastry, B.V.S., Habeeb, M.A., Khan, A.A., Dhayal, M., 2017. Use of biocompatible sorafenib-gold nanoconjugates for reversal of drug resistance in human hepatoblatoma cells. Sci. Rep. 7 (1), 8539. https://doi.org/10.1038/s41598-017-08878-y.
Yasir, M., Chauhan, I., Zafar, A., Verma, M., Noorulla, K.M., Tura, A.J., Alruwaili, N.K., Haji, M.J., Puri, D., Gobena, W.G., Dalecha, D.D., Sara, U.V.S., Kumar, N., 2021. Buspirone loaded solid lipid nanoparticles for amplification of nose to brain efficacy: Formulation development, optimization by Box-Behnken design, in-vitro characterization and in-vivo biological evaluation. J. Drug Deliv. Sci. Technol. 61, 102164 https://doi.org/10.1016/j.jddst.2020.102164.
Yasir, M., Zafar, A., Noorulla, K.M., Tura, A.J., Sara, U.V.S., Panjwani, D., Khalid, M., Haji, M.J., Gobena, W.G., Gebissa, T., Dalecha, D.D., 2022a. Nose to brain delivery of donepezil through surface modified NLCs: Formulation development, optimization,

and brain targeting study. J. Drug Deliv. Sci. Technol. 75, 103631 https://doi.org/10.1016/j.jddst.2022.103631.

Yasir, M., Chauhan, I., Zafar, A., Verma, M., Alruwaili, N., Noorulla, K.M., Singh, A., Tura, A., 2022b. Glyceryl behenate-based solid lipid nanoparticles as a carrier of haloperidol for nose to brain delivery: formulation development, in-vitro, and in-vivo evaluation. Braz. J. Pharm. Sci. 58 https://doi.org/10.1590/s2175-97902022e20254.

Zafar, A., Alsaidan, O.A., Imam, S.S., Yasir, M., Alharbi, K.S., Khalid, M., 2022a. Formulation and evaluation of moxifloxacin loaded bilosomes in-situ gel: optimization to antibacterial evaluation. Gels. 8 (7), 418. https://doi.org/10.3390/gels8070418, 4.

Zafar, A., Imam, S.S., Alruwaili, N.K., Yasir, M., Alsaidan, O.A., Alshehri, S., Ghoneim, M. M., Khalid, M., Alquraini, A., Alharthi, S.S., 2022b. Formulation and evaluation of topical nano-lipid-based delivery of butenafine: in vitro characterization and antifungal activity. Gels 8 (2), 133. https://doi.org/10.3390/gels8020133.